

Article

Electronic Structure, Spectroscopy, Cold Ion–Atom Elastic Collision Properties, and Photoassociation Formation Prediction of the $(\text{MgCs})^+$ Molecular Ion

Mohamed Farjallah ^{1,†}, Dibyendu Sardar ^{2,†}, Bimalendu Deb ² and Hamid Berriche ^{1,3,*} 

¹ Laboratory of Interfaces and Advanced Materials, Faculty of Sciences of Monastir, University of Monastir, Monastir 5019, Tunisia; farjallah_mohamed@yahoo.fr

² School of Physical Sciences, Indian Association for the Cultivation of Science (IACS), Jadavpur, Kolkata 700032, India; chem.dibyandu.sardar@gmail.com (D.S.); msbd@iacs.res.in (B.D.)

³ Department of Mathematics and Natural Sciences, School of Arts and Sciences, American University of Ras Al Khaimah, Ras Al-Khaimah P.O. Box 10021, United Arab Emirates

* Correspondence: hamid.berriche@aurak.ac.ae

† These authors contributed equally to this work.

Abstract: In this paper, we extensively study the electronic structure, interactions, and dynamics of the $(\text{MgCs})^+$ molecular ion. The exchanges between the alkaline atom and the low-energy cationic alkaline earths, which are important in the field of cold and ultracold quantum chemistry, are studied. We use an ab initio approach based on the formalism of non-empirical pseudo-potential for Mg^{2+} and Cs^+ cores, large Gaussian basis sets, and full-valence configuration interaction. In this context, the $(\text{MgCs})^+$ cation is treated as an effective two-electron system. Adiabatic potential energy curves and their spectroscopic constants for the ground and the first 20 excited states of $^{1,3}\Sigma^+$ symmetries are determined. Furthermore, we identify the avoided crossings between the electronic states of $^{1,3}\Sigma^+$ symmetries. These crossings are related to the charge transfer process between the two ionic limits, Mg/Cs^+ and Mg^+/Cs . Therefore, vibrational-level spacings and the transition and permanent dipole moments are presented and analyzed. Using the produced potential energy data, the ground-state scattering wave functions and elastic cross-sections are calculated for a wide range of energies. In addition, we predict the formation of a translationally and rotationally cold molecular ion $(\text{MgCs})^+$ in the ground-state electronic potential energy through a stimulated Raman-type process aided by ion–atom cold collision. In the low-energy limit (<1 mK), elastic scattering cross-sections exhibit Wigner law threshold behavior, while in the high-energy limit, the cross-sections act as a function of energy E go as $E^{-1/3}$. A qualitative discussion about the possibilities of forming cold $(\text{MgCs})^+$ molecular ions by photoassociative spectroscopy is presented.

Keywords: pseudo-potentials; configuration interaction; potential energy curves; spectroscopic constants; dipole moments; photoassociation; STIRAP



Citation: Farjallah, M.; Sardar, D.; Deb, B.; Berriche, H. Electronic Structure, Spectroscopy, Cold Ion–Atom Elastic Collision Properties, and Photoassociation Formation Prediction of the $(\text{MgCs})^+$ Molecular Ion. *Atoms* **2023**, *11*, 121. <https://doi.org/10.3390/atoms11090121>

Academic Editor: Yew Kam Ho

Received: 15 May 2023

Revised: 7 August 2023

Accepted: 11 August 2023

Published: 15 September 2023



Copyright: © 2023 by the authors. Licensee MDPI, Basel, Switzerland. This article is an open access article distributed under the terms and conditions of the Creative Commons Attribution (CC BY) license (<https://creativecommons.org/licenses/by/4.0/>).

1. Introduction

In recent years, cold and ultracold molecules [1] have received considerable attention owing to successful demonstrations of cooling and trapping of molecules [2] and their importance in high-resolution spectroscopy [3]. Due to the characteristics of long-range ion–atom potential, ion–neutral collisions [4–6] are different from neutral–neutral and ion–ion collisions. The long-range ion–atom potential is described by $-C_4/r^4$, where $C_4 = \alpha q^2 / (8\pi\epsilon_0)$, α is the static electric polarizability of the atom, r is the ion–atom separation, q is the charge of the ion, and ϵ_0 is the permittivity of free space. The scattering caused by this potential offers the main channel for the exchange of energy between the ions and the atoms. Accordingly, research on low-energy ion–neutral-atom collisions is very useful for the study of the sympathetic cooling of the translational motion of atomic

ions [7,8] and for obtaining precise control of the internal degrees of freedom and external molecular ions [9]. In addition, interactions between the alkali atoms and alkaline earth ions (Be^+ , Mg^+ , Sr^+ , and Ca^+) offer opportunities for new developments in the field of ultracold quantum matter, with the benefit of simpler and more reliable trapping compared to neutral molecules. Furthermore, a multitude of cold molecular ion species could be created, paving the way for rich chemistry at temperatures of a few mK or less [10]. The collision between cold atoms and ions is also relevant for important applications related to molecule formation in Bose–Einstein condensates [11] and quantum information. Photoassociation [12] and Feshbach resonance tuning [13] are two main experimental techniques for the coherent production of ultracold molecules from atoms.

Radiative emission during cold collisions between trapped laser-cooled Rb atoms and the alkaline earth ions Ca^+ , Sr^+ , and Ba^+ has been studied theoretically by Aymar et al. [14] using an effective core potential based on quantum chemistry calculations of potential energy curves and transition dipole moments of the related molecular ions. Furthermore, many experimental groups have carried out experiments with various combinations of alkali atoms and alkaline earth atomic ions: Rb atoms with Ca^+ [15,16] and Ba^+ [17] ions. Moreover, recently, other groups have studied the energy scaling of the cold-atom–atom–ion three-body recombination $\text{Ba}^+ + \text{Rb} + \text{Rb}$ in the mK regime where a single $^{138}\text{Ba}^+$ ion in a Paul trap is immersed in a cloud of ultracold ^{87}Rb atoms [18], as well as the life and death of a cold BaRb^+ molecule inside an ultracold cloud of Rb atoms [18]. In addition, an optical dipole trap of Rb atoms has also been merged in a Paul trap containing a few Ba^+ atoms [18].

Concerning MgH^+ , the first evidence of the formation of molecular MgH^+ ions in a laser-cooled ion trap was reported by Baba and Waki [19], who introduced air into an Mg^+ trap. Drewsen and colleagues [20] carried out a more controlled experiment, introducing a thermal gas H_2 or D_2 into a laser-cooled Mg^+ trap, thereby creating trapped MgH^+ or MgD^+ ions. Many other studies concerning magnesium hydride investigated its photodissociation [21], branching ratios [21], etc. More recently, Aymar et al. [22] carried out a study of the electron structure of the MgH^+ ionic molecule containing potential energy curves, transition and permanent dipole moment spectra, and static polarizabilities. Using an ab initio approach, Khemeri et al. [23] performed a study of the electronic properties of this molecule in the adiabatic representation.

Concerning the MgLi^+ ionic molecule, Boldyrev et al. [24] determined its ground-state spectroscopic constants using the split-valence basis MP2/6-311+G*. Pyykkö [25] employs two methods—Hartree–Fock (HF/6-31G*) and Møller–Plesset (MP)—to calculate the equilibrium distance, well depth, and vibration frequency for the same states. More recently, Yufeng Gao and Tao Gao [26] applied the ab initio program package MOLPRO to determine the potential energy curves and the permanent and transition dipole moments of the same molecules. They used the multireference configuration interaction and valence full-configuration interaction with large aug-cc-pCVQZ basis sets, taking into account the core–valence and scalar relativistic corrections.

A review of the scientific literature shows that experimental studies on the $(\text{MgCs})^+$ [27] cationic molecule are practically absent. We only noticed the existence of one recent theoretical study of $(\text{MgCs})^+$, in which the authors Smialkowski and Tomza [28] only reported spectroscopic constants for the ground state. Therefore, a more detailed and refined investigation of this molecular system is desirable. Methods fundamentally similar to those used for the treatment of the $(\text{MgLi})^+$ molecule [29,30] will be employed in the present study.

Several groups in the world have experimentally investigated atom–ion and cold molecular diatomic mixtures. The list of such mixtures includes Yb_2^+ [31], RbCa^+ [16], CaBa^+ [32], CaYb^+ [33], RbYb^+ [34], LiCa^+ [35], RbCa^+ [15], NaCa^+ [36], RbSr^+ [37], LiYb^+ [38], KCa^+ [39], RbBa^+ [40], Rb_2^+ [41,42], and BaRb^+ [43], as well as homonuclear mixtures [44]. Alkaline earth ions are a common choice as advanced methods for manipulation and detection of such ions have been developed over the years, creating prospects for their applications in quantum simulation and computations [45,46]. Atom–ion diatomic

molecular systems can be produced via cold collision-induced charge-transfer radiative association, light-induced photoassociation [47–51], or photoionization of ultracold neutral molecules [42,44]. The effective core potential methods followed by CI and quantum chemistry calculations are employed to calculate the potential energy curves and dipole moments. In a very recent work [52] by our group, we investigated the electronic structure of the five diatomic molecular ions composed of a Ca^+ ion interacting with an alkali metal atom: CaX^+ ($X = \text{Li, Na, K, Rb, Cs}$). Also, the molecular ion structure of BeX^+ ($X = \text{Na, K, Rb}$) systems has been theoretically studied [53], and the forming of a cold ion–atom mixture by stimulated Raman adiabatic process has been investigated [54]. In addition, an extensive study of the electronic structure, the cold ion–atom elastic collision properties, and the possibility of laser cooling BeCs^+ molecular ions has recently been investigated [55].

Very recently, Smialkowski et al. theoretically investigated the ground-state electronic structure of single-charged molecular ions formed from two or three interacting alkali metal and alkaline earth metal atoms. They calculated the ground-state electronic properties of all diatomic AB^+ and most of the triatomic A_2B^+ molecular ions consisting of Li, Na, K, Rb, Cs, Mg, Ca, Sr, Ba, and Yb atoms. Smialkowski and Tomza [28] carried out a systematic study of the electronic structure of MgX^+ ($X = \text{Li, Na, K, Rb}$ and Cs) ionic systems and presented the potential energy curves and spectroscopic constants for their ground states.

Here, we investigate the adiabatic potential energy curves for many electronic states of $1,3\Sigma^+$, $1,3\Pi$, and $1,3\Delta$ symmetries below the $\text{Mg}^{2+}\text{Cs}^-$ asymptotic limit. Then, we extract the spectroscopic constants from these curves (equilibrium distance R_e , well depth D_e , electronic excitation energy T_e , frequency ω_e , harmonicity constant $\omega_e x_e$, and rotational constant B_e). In addition, vibrational-level spacings and the dipole moment function are also presented and analyzed. By exploiting the ab-initio potential energy data, we study elastic collisions between an alkali ion Cs^+ and a neutral alkaline earth atom Mg for the ground-state collisional threshold. Besides that, we predict and analyze the formation of translationally and rotationally cold molecular ions by a two-photon incoherent Raman process in the presence of two applied lasers.

This paper is organized as follows. In Section 2, the methodology used is briefly presented. We report our results for $(\text{MgCs})^+$ and discuss them in Section 3.

2. Theory and Computational Details

In this section, we give an overview of the technical details of the calculation of the $(\text{MgCs})^+$ molecular ion. Numerous studies on heteronuclear alkaline earth dimers such as $(\text{MgK})^+$ [49], $(\text{BeLi})^+$ [56], $(\text{BeH})^+$ [57], $(\text{CaRb})^+$, $(\text{SrRb})^+$, and $(\text{BaRb})^+$ [15] have been performed. We used the CIPSI package (Configuration Interaction by Perturbation of a Multi-configuration Wave Function Selected Iteratively) of the Laboratoire de Physique et Chimie Quantique of Toulouse in France [58]. The ionic system $(\text{MgCs})^+$ has 67 electrons. Therefore, we replaced the cores of the Mg^{2+} (10 electrons) and Cs^+ (54 electrons) with non-empirical pseudo-potentials proposed by Barthelat and Durand [59–61]. Consequently, $(\text{MgCs})^+$ is treated as an effective two-electron system, where the two valence electrons are moving in the field of the two cores. The pseudo-potential is complemented by the corrections of core–core and core–valence correlations according to the operator formalism of Muller et al. [62]. In addition, the cut-off function reported by the formulation of Foucault et al. [63] is taken to be a function of l , the orbital angular momentum, in order to treat separately the interaction of valence electrons of different spatial symmetry and the core electrons. The cut-off radii for the lowest valence s, p, d, and f one-electron states are reported in Table 1.

Table 1. Polarizabilities, cut-off radii, and pseudo-potential parameter (in a.u.) atoms.

Atom	α	ρ_s	ρ_p	ρ_d
Mg($Z = 12$)	0.46904	0.9	1.25499	1.500
Cs($Z = 55$)	15.117	2.69	1.85	2.810

In the present work, the core polarizabilities are taken to be $0.46904 a_0^3$ [63] for Mg^{2+} and $15.117a_0^3$ [64,65], respectively. For magnesium, we used a large Gaussian basis set (9s, 7p, 5d, and 4f) composed of 83 functions. The diffuse orbital exponents have been optimized to reproduce (with good accuracy) all atomic states dissociating into the following: Mg^+ (3s, 3p, 4s, 3d, 4p, 5s, 4d, 4f, 5p, and 6s) and Mg ($3s^2$ (1S), $3s3p$ (3P), $3s3p$ (1P), $3s4s$ (3S), $3s4s$ (1S), $3s3d$ (1D), $3s4p$ (3P), $3s3d$ (3D), $3s4p$ (1P), $3s5s$ (3S), $3s5s$ (1S), $3s4d$ (1D), $3s4d$ (3D), and $3s5p$ (3P)). After contraction, this basis was reduced to 7s/7p/4d/4f, and the function number decreased to only 76. Aymar et al. [22] used a (7s/5p/4d/2f) basis set contracted to (6s/5p/2d/2f); therefore, the function number decreases from 56 to 45, while for Cs, we used a (7s4p5d1f/6s4p4d) Gaussian basis set taken from [22,66]. Molecular energies for $(\text{MgCs})^+$, at the dissociation limits, are given in Table 2.

The quality of the used basis sets and cut-off radii is confirmed by the good agreement between our values and the experimental [67] and theoretical [68,69] atomic energy levels. The difference between our results and the experimental values for almost all energy levels is lower than 179 cm^{-1} , which is found for the Mg (3s4s) atomic level. However, a difference of 1445 cm^{-1} is found for the Mg (3s3d) atomic level. Nevertheless, the agreement between the energy levels of Mg^+ and the experimental ones is much better, seeing that we have reproduced Mg^+ experimental binding energies exactly for 3s, 3p, 3d, and 4p. The difference with experimental values for the Mg^+ (4s) atomic level is equal to 1.53 cm^{-1} , and for the other highly excited states 5s, 4d, 4f, 5p, and 6s, the discrepancy is between 22 and 105 cm^{-1} .

Table 2. Asymptotic energy of the alkali earth $(\text{MgCs})^+$ electronic states (in cm^{-1}): comparison between our calculated energy, Moore et al.'s [70] calculated energy, and the corresponding experimental dissociation.

State	Asymptotic Molecular State	This Work	Experiment [68,70]
X (1) $^1\Sigma^+$	Mg ($3s^2$) + Cs ⁺	0	0
A (2) $^1\Sigma^+$	Mg^+ (3s) + Cs (6s)	30,263.62	30,398.60
C (3) $^1\Sigma^+$	Mg (3s3p) + Cs ⁺	35,050.59	35,319.67
D (4) $^1\Sigma^+$	Mg^+ (3s) + Cs (6p)	41,811.30	41,946.72
E (5) $^1\Sigma^+$	Mg (3s4s) + Cs ⁺	43,502.57	43,472.29
F (6) $^1\Sigma^+$	Mg^+ (3s) + Cs (5d)	44,821.40	44,956.60
G (7) $^1\Sigma^+$	Mg (3s3d) + Cs ⁺	46,402.50	47,967.79
H (8) $^1\Sigma^+$	Mg^+ (3s) + Cs (7s)	48,802.02	48,934.58
I (9) $^1\Sigma^+$	Mg (3s4p) + Cs ⁺	49,346.10	49,487.00
J (10) $^1\Sigma^+$	Mg^+ (3s) + Cs (7p)	52,143.74	52,284.65
a (1) $^3\Sigma^+$	Mg (3s3p) + Cs ⁺	21,876.60	21,994.46
c (2) $^3\Sigma^+$	Mg^+ (3s) + Cs (6s)	30,263.62	30,398.60
d (3) $^3\Sigma^+$	Mg (3s4s) + Cs ⁺	41,196.77	41,154.85
e (4) $^3\Sigma^+$	Mg^+ (3s) + Cs (6p)	41,811.30	41,946.72
f (5) $^3\Sigma^+$	Mg^+ (3s) + Cs (5d)	44,821.40	44,956.60
g (6) $^3\Sigma^+$	Mg (3s4p) + Cs ⁺	47,857.84	48,197.80
h (7) $^3\Sigma^+$	Mg (3s3d) + Cs ⁺	47,956.38	46,647.87
I (8) $^3\Sigma^+$	Mg^+ (3s) + Cs (7s)	48,802.02	48,934.58
J (9) $^3\Sigma^+$	Mg (3s5s) + Cs ⁺	51,871.81	51,976.72
k (10) $^3\Sigma^+$	Mg^+ (3s) + Cs (7p)	52,143.74	52,284.65

2.1. Results and Discussions

2.1.1. Adiabatic Potential Energy and Spectroscopic Constants

Using the method reported in the previous section, a full and expanded calculation was performed for many electronic states of $^1,3\Sigma^+$, symmetries for the $(\text{MgCs})^+$ cationic molecule. These states dissociate into Mg^+ (3s, 3p, 4s, 3d, 4p, 5s, 4d, 4f, 5p, and 6s) + Cs (6s, 6p, 4d, 5d, 7s, and 7p) and Mg $\{(3s^2$ (1S), $3s3p$ (3P), $3s3p$ (1P), $3s4s$ (3S), $3s4s$ (1S), $3s3d$ (1D), $3s4p$ (3P), $3s3d$ (3D), (1P), $3s5s$ (3S), $3s5s$ (1S), $3s4d$ (1D), $3s4d$ (3D), and $3s5p$ (3P))} + Cs⁺.

The adiabatic potential energy is performed for an interval of intermolecular distances from 3.50 to 200.00 a_0 with a step of 0.1 a_0 around the avoided crossings. The potential energy curves as functions of the internuclear distance R for the $1,3\Sigma^+$ electronic states are drawn, respectively, in Figures 1 and 2.

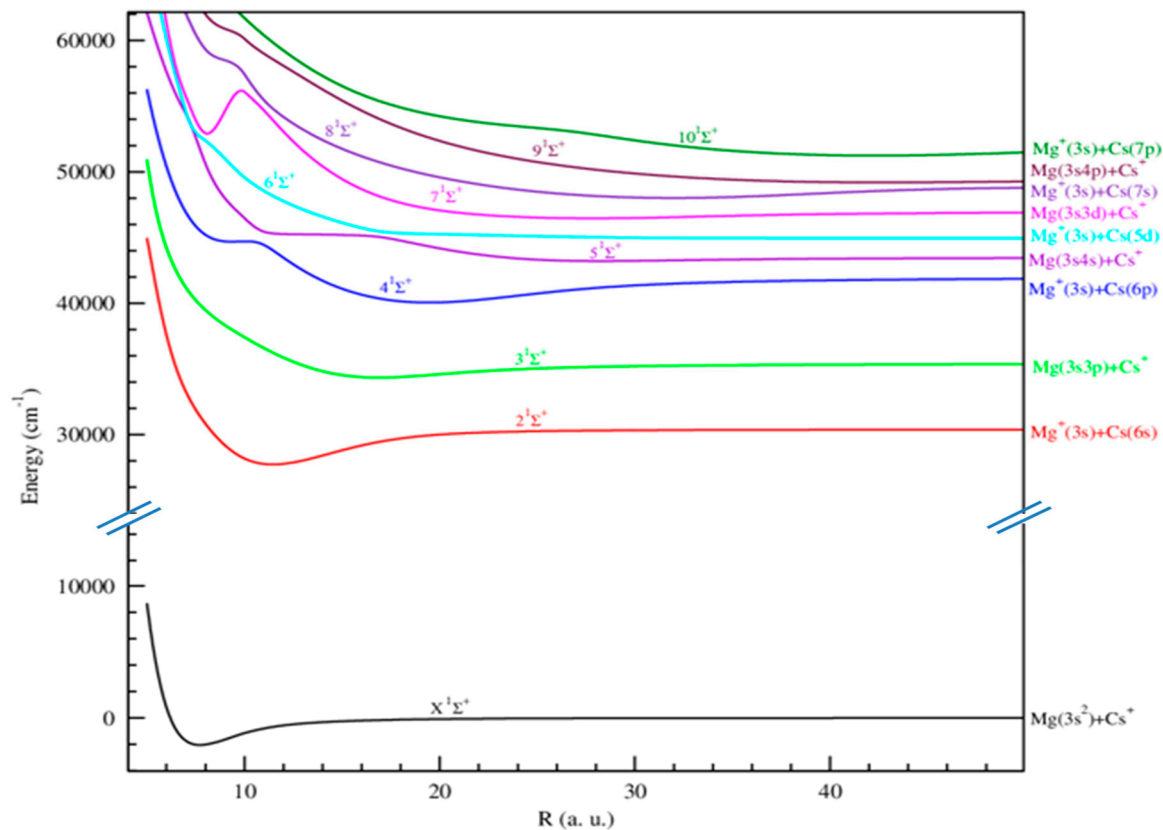


Figure 1. Adiabatic potential energy curves of the first $10^1\Sigma^+$ electronic states of $(\text{MgCs})^+$.

In order to assess the precision of our calculated potential energy curves for the states previously studied, we have extracted the spectroscopic constants (equilibrium distance R_e , well depth D_e , electronic excitation energy T_e , frequency ω_e , harmonicity constant $\omega_e x_e$, and rotational constant B_e for the equilibrium separation R_e). These constants were determined by least-squares interpolation of the vibrational energy levels. Unfortunately, no experimental spectroscopic information for $(\text{MgCs})^+$ has been published yet. However, Smialkowski and Tomza [28] reported a theoretical calculation for the ground state. They found $R_e = 7.85 a_0$, $D_e = 1861 \text{ cm}^{-1}$, $\omega_e = 73.2 \text{ cm}^{-1}$, and $B_e = 0.0481 \text{ cm}^{-1}$, which are close to our values ($R_e = 7.70 a_0$, $D_e = 2047 \text{ cm}^{-1}$, $\omega_e = 73.2 \text{ cm}^{-1}$, and $B_e = 0.049364 \text{ cm}^{-1}$) (see Table 3). Therefore, the spectroscopic constants for the excited states are presented here for the first time. Consequently, we think that these potential energies and spectroscopic data can initiate future experimental and theoretical investigations on this molecular ionic system. In Table 3, we report the spectroscopic constants for the ground and the excited states for all symmetries.

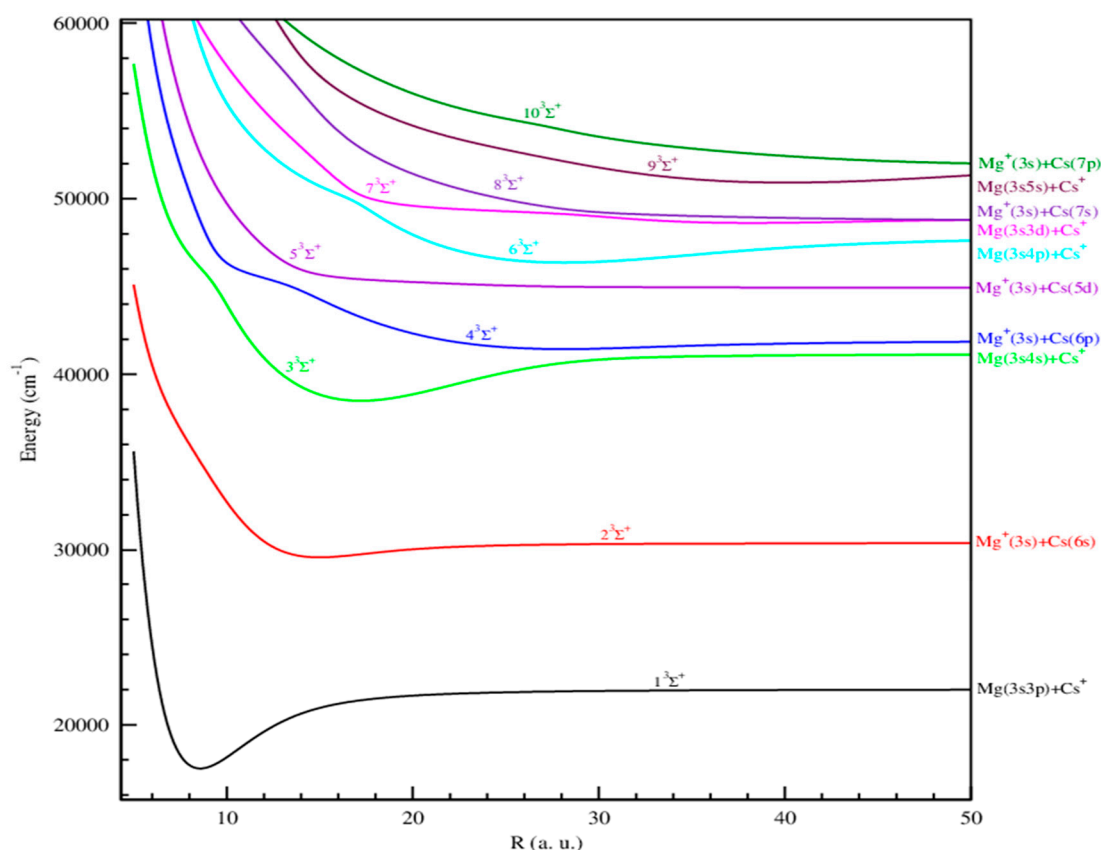


Figure 2. Adiabatic potential energy curves of the first $10^3\Sigma^+$ electronic states of $(\text{MgCs})^+$.

The potential energy curves for the 20 first $1,3\Sigma^+$ states of $(\text{MgCs})^+$ molecular ion are plotted in Figures 1 and 2. These states are labelled by increasing numbers from 1 to 10 for both singlet and triplet states

The ground ($X^1\Sigma^+$) and the first excited ($2^1\Sigma^+$) states are well separated from the highest states of the same symmetry, and they maintain an energy gap of about $42,012\text{ cm}^{-1}$. Both are found with unique minimums at 7.7 and 11.45 a_0 and well depths of 2047 and 2662 cm^{-1} , respectively. The first three excited triplet states $(1-3)^3\Sigma$ also exhibit unique minimums at 8.58, 14.98, and 17.20 a_0 , with significant well depths of 4504, 813, and 2658 cm^{-1} , respectively. An accurate analysis of these curves shows that the most strongly bound states are the first excited states of both singlet and triplet states with well depths of 2662 and 4504 cm^{-1} located at 11.45 and 8.58 a_0 , respectively.

An interesting feature of the higher excited states of all symmetries of $1,3\Sigma^+$ states has been noticed. The shape becomes more involved, with double wells and potential barriers. This feature is due to the presence of many avoided crossings at short and large values of internuclear distances between excited states of the same symmetries. The positions of such avoided crossings are presented in Figures 1 and 2. These series of avoided crossings are related to underlying charge transfer between the ionic configurations Mg^+/Cs and Mg/Cs^+ . Later, these avoided crossings will be discussed in light of the behavior of the permanent dipole moments.

The PECs of excited states starting from $4^1\Sigma^+$ present double wells and barriers, which are the consequence of avoiding crossings that happen at specific internuclear distances. These avoided crossings are related to underlying charge transfer, as can be seen from the change of location of the positive charge at dissociation limits between two neighbor states. The positive charge moves from one atom to the second one. The existence of these avoided crossings will generate large nondiabatic couplings. This same behavior has been seen for other symmetries, such as $3\Sigma^+$ states.

Table 3. Spectroscopic constants of the ground and excited singlet and triplet electronic states of (MgCs)⁺ molecule.

State	R _e (a.u.)	D _e (cm ⁻¹)	T _e (cm ⁻¹)	ω _e (cm ⁻¹)	ω _e x _e (cm ⁻¹)	B _e (cm ⁻¹)
χ ¹ Σ ⁺	7.70	2047	0	73.2	0.63	0.049364
	7.85 [28]	1861 [28]		73.2 [28]	0.0481 [28]	
2 ¹ Σ ⁺	11.45	2662	29,782	44.64	0.25	0.022354
3 ¹ Σ ⁺	16.88	1054	36,391	21.92	0.16	0.010280
4 ¹ Σ ⁺	9.33	−2750				
	19.46	1891	42,101	21.73	0.06	0.007700
5 ¹ Σ ⁺	28.24	263	45,256	9.12	0.07	0.003674
6 ¹ Σ ⁺	58.89	4	46,990	−0.48	14.61	0.001160
7 ¹ Σ ⁺	8.68	−3301				
	27.83	509	48,507	8.92	26.51	0.038919
8 ¹ Σ ⁺	8.68	−8647				
	31.99	923	50,059	10.13	29.95	0.038864
9 ¹ Σ ⁺	8.69	−10,460				
	42.75	300	51,240	5.44	30.84	0.038839
10 ¹ Σ ⁺	8.71	−10,297				
	42.27	1105	53,289	8.07	40.10	0.038614
1 ³ Σ ⁺	8.58	4504	19,556	74.78	0.52	0.039826
2 ³ Σ ⁺	14.98	813	31,630	25.56	0.17	0.013050
3 ³ Σ ⁺	17.20	2658	40,542	26.85	0.05	0.009905
4 ³ Σ ⁺	28.15	506	43,486	10.12	0.04	0.003698
5 ³ Σ ⁺	58.89	4	46,990	−0.48	14.61	0.001160
6 ³ Σ ⁺	28.13	1600	48,413	13.19	0.02	0.003704
7 ³ Σ ⁺	38.20	31	50,667	6.81	0.03	0.002008
8 ³ Σ ⁺	49.32	131	50,850	4.59	0.02	0.001205
9 ³ Σ ⁺	40.09	1055	52,967	8.79	0.01	0.001823
10 ³ Σ ⁺	56.76	395	53,999	3.95	0.01	0.000910

2.1.2. Vibrational Levels

For a better understanding of the potential energy curve structure, the vibrational levels for all attractive states are computed using the Numerov algorithm. The interpolation of the potential curves is carried out with 12,000 points and a grid ranging from 3.5 to 180.0 a₀.

The vibrational spacings (E_{v+1}−E_v) as a function of the vibrational quantum number v are reported in Figure 3 for the ^{1,3}Σ⁺ states. As usual, these spacings are not constant due to the important anharmonicity observed in the potential energy curves. The number of the vibration levels for the ground and the first excited states are 80 and 180, respectively. The vibrational energy spacing of these two potentials shows a linear behavior for low vibrational levels, and then it vanishes at the dissociation limits.

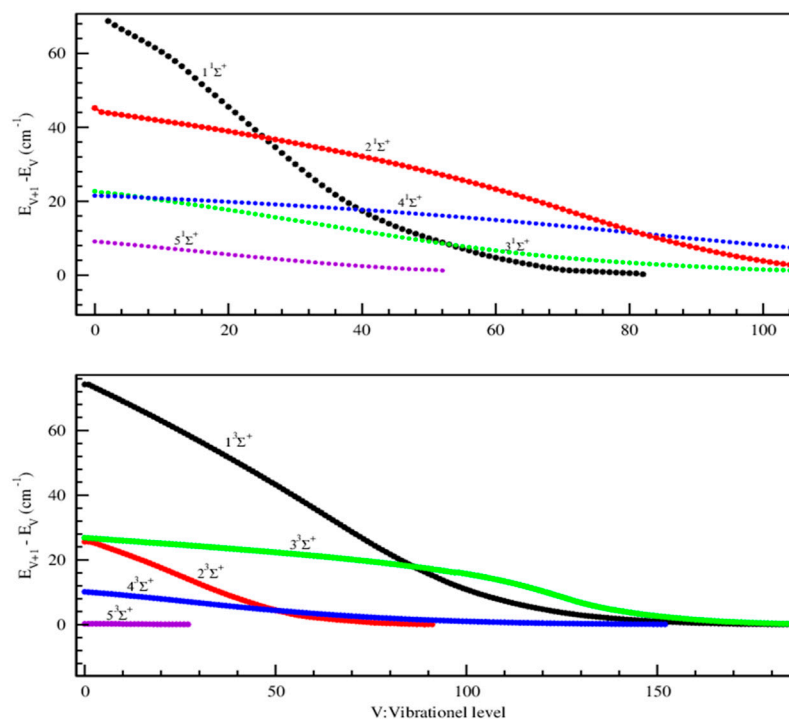


Figure 3. Vibrational energy level spacing ($E_{(v+1)} - E_{(v)}$) (in cm^{-1}) for the ($1,3\Sigma^+$) electronic states of the $(\text{MgCs})^+$ molecule.

The spacing between vibrational levels decreases gradually as vibrational energy increases. This behavior is particularly prominent for vibrational levels of the PECs that reflect the strong anharmonicity. The overall pattern of energy spacings of different electronic states of the molecular ion is similar. However, for some states, irregularities related to the avoided crossings are visible, e.g., for the $1^1\Sigma^+$ states.

2.1.3. Permanent and Transition Dipole Moments

In addition to the potential energy curves, the practical implementation of cold molecule formation via photoassociation requires knowledge of their electronic properties, such as the radial variation of permanent or transition dipole moments. Furthermore, the knowledge of the dipole function of molecular systems can be considered a sensitive test for the accuracy of the calculated electronic wave functions and energies.

Keeping this broad perspective of the ion–atom systems in mind, we have determined the permanent and transition dipole moments for the same large and dense grid of internuclear distances used for the potential energy curves.

Permanent Dipole Moments

The permanent and transition dipole moments are determined by considering the origin at atom Mg, and where the distance R between Mg/Mg^+ and Cs/Cs^+ stands for the internuclear distance between them. We calculated the permanent dipole moments as a function of R ; the intermolecular distance for all studied states ($1-10^1\Sigma^+$, $1-10^3\Sigma^+$) are displayed in Figures 4 and 5.

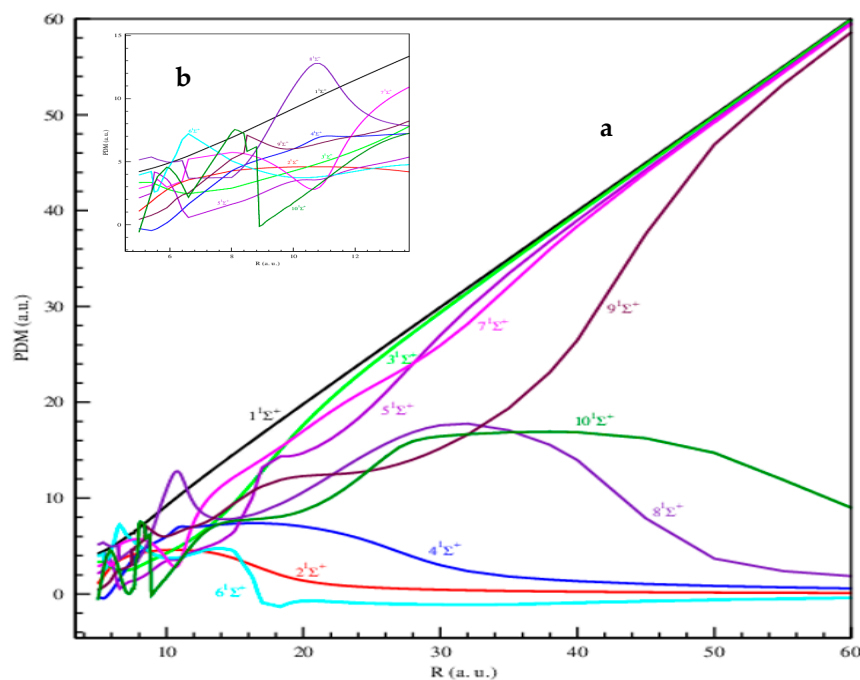


Figure 4. (a) Permanent dipole moment for the $1\Sigma^+$ states of the $(\text{MgCs})^+$ molecular ion. (b) Zoomed area at distances between 0 and 15 a.u.

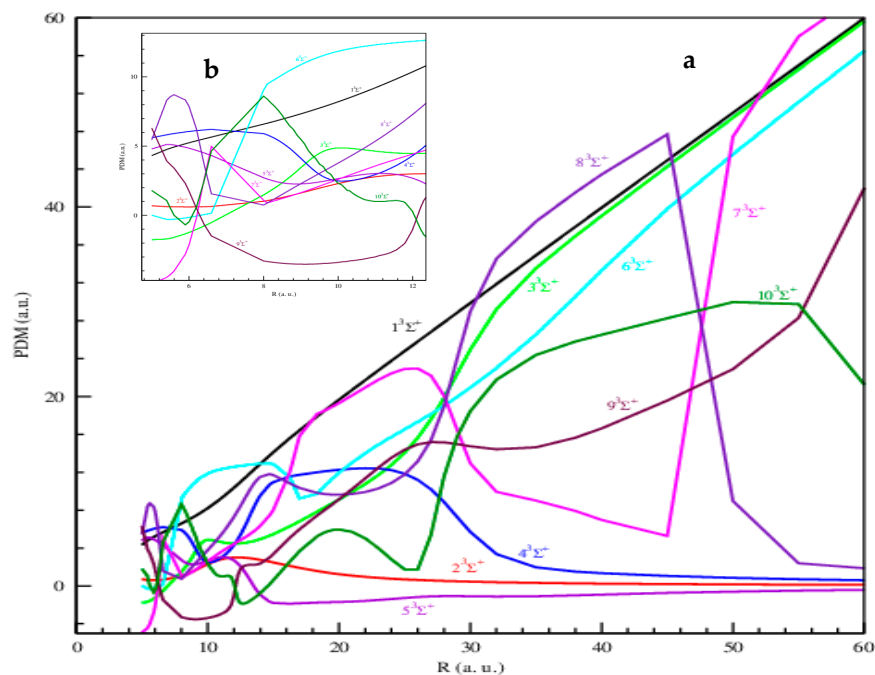


Figure 5. (a) Permanent dipole moment for the $3\Sigma^+$ states of the $(\text{MgCs})^+$ molecular ion. (b) Zoomed area at distance between 0 and 15 a.u.

At a short and intermediate internuclear distance, the permanent dipole moments present undulations with abrupt variation between neighbor electronic states. For example, there is an abrupt variation between the $8^1\Sigma^+$ and $9^1\Sigma^+$ states located at $33.5 a_0$. We remark that this particular distance represents approximately the position of the avoided crossing between the two potential energy curves that we noticed before. We can conclude that the significant changes in permanent dipole moment at a small internuclear distance are due to the change in the polarity of the molecule. In addition, the positions of the irregularities in

the R-dependence of the permanent dipole are correlated to the avoided crossings between potential energy curves, which are both manifestations of abrupt changes in the character of the electronic wave functions.

For the large internuclear distance, the permanent dipole moment of the $X^1\Sigma^+$, $3^1\Sigma^+$, $5^1\Sigma^+$, $7^1\Sigma^+$, and $9^1\Sigma^+$ states dissociating into Mg ($3s^2, 3s3p, 3s3p, 3s4s, 3s4s, 3s3d, 3s4p, 3s3d, 3s5s, 3s5s, 3s4d, 3s4d, \text{ and } 3s5p$) + Cs^+ are significant and yield a pure linear behavior function of R, especially at intermediate and large distances. For the remaining states $2^1\Sigma^+$, $4^1\Sigma^+$, $6^1\Sigma^+$, and $10^1\Sigma^+$ dissociating into Mg^+ ($3s, 3p, 4s, 3d, 4p, 5s, 4d, 4f, 5p, \text{ and } 6s$) + Cs ($6s, 6p, 4d, 5d, 7s \text{ and } 7p$), we note significant permanent dipole moments in specific regions and then they vanish swiftly at large distances.

For the permanent dipole moments of the first ten states of $^3\Sigma^+$ symmetry, similar observations were noticed as for the $^1\Sigma^+$ states. They exhibit undulations with abrupt variations at a short and intermediate internuclear distance R, such as between the two states $8^3\Sigma^+$ and $9^3\Sigma^+$ around $27.7 a_0$. We remark that the permanent dipole moments of these states, one after another, behave in a straight line on the same curve and then drop to zero at particular distances corresponding to the avoided crossings between neighboring electronic states.

Transition Dipole Moments

In addition, we have determined the transition dipole moment functions for the $(MgCs)^+$ ionic molecular system between states of similar symmetries. As the transition dipole moments between adjacent states are the most significant, here, we only present the transition between neighbor states. They are displayed in Figure 6.

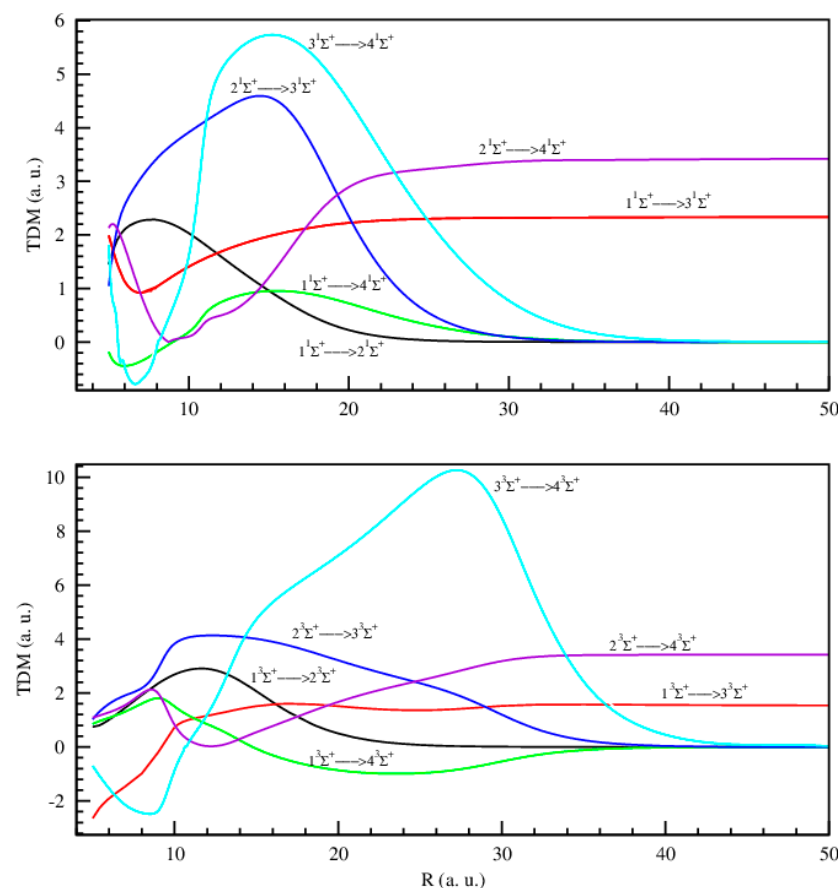


Figure 6. Transition dipole moments for selected (1- \rightarrow 2, 2- \rightarrow 3, and 3- \rightarrow 4) $^1,3\Sigma^+$ states as a function of the internuclear distance R.

Theoretically, Fedorov et al. [27] reported dipole moments for the molecular ions (MgLi)⁺ and (MgNa)⁺. They have calculated the transition dipole moments for the latter systems; however, no data for the (MgCs)⁺ ionic molecule are available, and these important physical quantities are presented here for the first time. We note a meaningful variation with numerous extremum, which can be assigned to avoid crossing positions between adjacent states. We also note a change in the sign of some dipole transitions, such as between 3¹Σ⁺->4¹Σ⁺ states. This change in sign corresponds to a sudden change in electronic wave functions, which is usually related to the avoided crossings between the potential energy curves.

For the triplet sigma states, the transition dipole moment curves between the neighbor states are displayed in Figure 6. We note similar behaviors observed previously for the singlet states. For both multiplicities, ^{1,3}Σ states, the weakly avoided crossing series already found between neighboring states lead to abrupt variations in the transition dipole moments.

2.1.4. Radiative Lifetime

In this section, we present the vibrational state lifetimes for A¹Σ⁺ (2¹Σ⁺) excited state. Given a vibrational level of the first excited electronic state, two possible transitions can occur: bound–bound and bound-free transitions. The radiative lifetime of a vibrational level corresponding to only bound–bound transitions is given by

$$\tau_{v'} = \frac{1}{\Gamma_{v'}} \text{ where } \Gamma_{v'} = \sum_{v=0}^{nv'} A_{vv'} \tag{1}$$

A_{vv'} is the Einstein coefficient linking, for example, the A¹Σ⁺(v') and X¹Σ⁺(v) levels. Zemke et al. [71] have previously shown that there is a missing contribution in the radiative lifetime. It corresponds to the bound-free transitions, which are more significant for the higher vibrational levels close to the dissociation limit of the excited electronic state, found in the form of the continuum radiation to states above the dissociation limit of the ground state. It corresponds to the contribution of the bound-free transition missed in Equation (1). It is related to the transition between the vibrational level v', which belongs to the excited electronic state, to the continuum of the ground state or the lower state in general. Such contribution is not negligible, as was demonstrated by Partridge et al. [72], Zemke et al. [71], and Berriche and Gadea [73,74]. It is more important for the higher vibrational levels due to the difference in the location of the potential wells. We calculate this contribution using two different approximations, “Franck-Condon” [72,73] and the “sum rule method” [72,75] approximation. In the Franck–Condon (FC) approximation proposed by Zemke et al. [71], the bound-free contribution is given by

$$A_{v'}(bound - free) = 2.14198639 \times 10^{10} |\mu(R_{v'+})|^2 FC_{v',cont}(\Delta E)^3_{v',cont} \tag{2}$$

where ΔE_{v',cont} = E_{v'} - E_{as} is the energy difference between the vibrational level v and the energy of the asymptotic limit of the lower electronic state to which the continuum belongs. The quantity μ(R_{v'+}) corresponds to the transition dipole moment at the right external turning point of the vibrational level v'.

$$FC_{v',cont} = \int |\langle \chi_{v'} | \chi_E \rangle|^2 dE = 1 - \sum_{v=0}^{nv'} |\langle \chi_{v'} | \chi_v \rangle|^2 \tag{3}$$

The approximate sum rule approach, implemented by Pazyuk et al. [76], allows the production of the radiative lifetime components for diatomic vibronic states, including the bound-free contribution. In addition, this approximation has a high efficiency for

non-diagonal systems, particularly for those with significant continuum contributions. The radiative lifetime using the sum rule method is given by

$$\frac{1}{\tau} = \int_{R_{\min}}^{R_{\max}} \phi_{v'}(R) \left(D(R^2) \right) \left(\Delta(R^3) \right) \phi_{v'}(R) dR \tag{4}$$

$\phi_{v'}(R)$ is the wave function of the vibrational level belonging to the $A^1\Sigma^+$ excited electronic state. $D(R)$ is the transition dipole moment between the ground $X^1\Sigma^+$ and the first excited $A^1\Sigma^+$ states. $\Delta U(R)$ is the energy difference between the ground $X^1\Sigma^+$ and the first excited $A^1\Sigma^+$ states. The total radiative lifetime, taking into account the bound-bound and bound-free contributions, using the two approaches, FC approximation and the approximate sum approach, are presented in Table 4.

Table 4. Radiative lifetimes and vibrational-level spacing $E_v - E_{v-1}$ of the $2^1\Sigma^+$ state of the $(MgCs)^+$ ion.

Vibrational Level	$E_v - E_{v-1}$ (cm ⁻¹)	Franck–Condon (ns)	Sum Rule (ns)
0		10.579	10.582
1	44.110	10.658	10.661
2	43.878	10.739	10.742
3	43.599	10.825	10.828
4	43.367	10.912	10.915
5	43.080	11.003	11.006
6	42.848	11.096	11.098
7	42.550	11.191	11.194
8	42.278	11.290	11.294
9	42.016	11.394	11.399
10	41.744	11.502	11.511
11	41.477	11.634	11.666
12	41.213	11.770	11.824
13	40.941	12.055	12.253
14	40.666	12.294	12.589
15	40.389	12.989	13.787
16	40.109	13.549	14.649
17	39.832	14.486	16.450
18	39.534	15.301	17.708
19	39.237	15.689	18.283
20	38.926	15.967	18.465
21	38.604	16.259	18.689
22	38.293	17.042	19.857
23	37.992	17.532	20.454
24	37.668	18.321	21.644
25	37.352	18.660	21.795
26	37.041	19.142	22.251
27	36.707	19.728	22.916
28	36.381	20.504	23.969
29	36.044	21.158	24.555
30	35.699	21.574	24.792
31	35.361	22.446	25.859
32	35.012	23.075	26.408
33	34.666	23.816	27.190
34	34.312	24.277	27.467
35	33.959	25.217	28.468
36	33.599	26.400	29.687
37	33.235	26.976	30.140
38	32.868	27.668	30.647
39	32.493	28.386	31.252
40	32.114	29.689	32.700

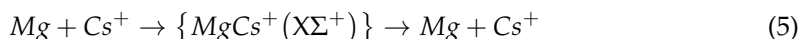
Table 4. *Cont.*

Vibrational Level	$E_v - E_{v-1}$ (cm ⁻¹)	Franck–Condon (ns)	Sum Rule (ns)
41	31.726	30.554	33.375
42	31.333	31.446	34.124
43	30.932	32.939	35.617
44	30.526	33.864	36.390
45	30.118	34.807	37.156
46	29.705	35.796	37.999
47	29.287	37.175	39.363
48	28.863	38.664	40.724
49	28.435	39.788	41.692
50	28.000	41.625	43.490

To the best of our knowledge, this is the first time that the radiative lifetimes of the vibrational levels of the $A^1\Sigma^+$ state of the $(MgCs)^+$ molecules have been presented. These radiative lifetimes increase with the vibrational level v in a range of 10–43 ns.

2.1.5. Ion–Atom Elastic Collisions

In this section, we study cold elastic collisions between an alkaline earth atom and an alkali ion in the ground electronic state ($X^1\Sigma^+$) of the $(MgCs)^+$ molecular system. The ground-state potential asymptotically correlates to the heavier alkali element in the ionic state (Cs^+) and the alkaline element in its neutral ground state (Mg). The first singlet excited state $2^1\Sigma^+$ asymptotically corresponds to the charge-exchanged state of the $X^1\Sigma^+$ potential. We use $Mg + Cs^+$ as a prototype system, and several results equally apply to other alkaline-earth-alkali atom–ion collisional systems. The elastic collisions between the alkaline earth atom, Mg, and alkali ion, Cs^+ , for the ground-state potential ($X^1\Sigma^+$) can be represented as



The partial-wave Schrödinger equation for the ion–atom elastic collision can be expressed as

$$\left[\frac{d^2}{dr^2} + k^2 - \frac{2\mu}{\hbar^2}V(r) - \frac{l(l+1)}{r^2} \right] \psi_l(kr) = 0 \tag{6}$$

where r is the internuclear separation between an atom and ion, μ is the reduced mass of an ion–atom colliding pair, and $\psi_l(kr)$ is the wave function for the l^{th} partial wave. The wave function satisfies the asymptotic boundary condition $\psi_l(kr) \sim \sin\left[kr - \frac{l\pi}{2} + \eta_l\right]$. The above second-order differential Equation 6 can be solved by the Numerov–Cooley algorithm [77] using three-point recursion relation. Initially, we set the values of the wave function at two initial consecutive points at small internuclear separation $r \sim 0$. Thereafter, the code calculates the wave function at the third point by utilizing the three-point recursion relation. Then, the second and third points are reset to the initial point, and the wave function is calculated for the fourth point. This process is continued until the asymptotic boundary is attained. The initial boundary conditions are included by expanding the interaction potential at small r and solving the Schrödinger equation at this limit. The boundary condition at the asymptotic limit is incorporated by setting the condition that the effective long-range part of potential $V(r)$ is much less than the collisional energy E (at least one-tenth of E). We considered a constant step size of 0.01 during the propagation of the code.

The total elastic scattering cross-section is given by

$$\sigma_{tot} = \frac{4\pi}{k^2} \sum_{l=0}^{\infty} (2l+1) \sin^2(\eta_l) \tag{7}$$

where k is the wave number related to the collisional energy $E = \frac{\hbar^2 k^2}{2\mu}$ and η_l being the phase shift for the l -th partial wave. As with an increase in energy, a large number of partial waves start to contribute to elastic scattering cross-section. Under this condition, the scattering cross-section is approximated as [4]

$$\sigma_{tot} \approx \pi \left(\frac{\mu C_4^2}{\hbar^2} \right)^{\frac{1}{3}} \left(1 + \frac{\pi^2}{16} \right) E^{-\frac{1}{3}} \tag{8}$$

The coefficient C_4 is related to the static electric dipole polarizability of the concerned atom.

But, at a very low energy limit, i.e., $E \rightarrow 0$, the phase shift follows the Wigner threshold laws. At this energy regime, the phase shift is related to the s -wave scattering length $a_s = -\lim_{k \rightarrow 0} \frac{\tan \eta_0}{k}$. The scattering length carries the information about the interaction potential of a system. A positive (negative) scattering length is associated with repulsive (attractive) interaction.

In Figure 7, we show the logarithm of total elastic scattering cross-sections (σ_{tot}) in a.u. as a function of the logarithm of energy E in K for ground-state collisions between neutral alkaline earth atom Mg and alkali ion Cs^+ . In order to calculate the convergence results in σ_{tot} , we need 59 partial waves.

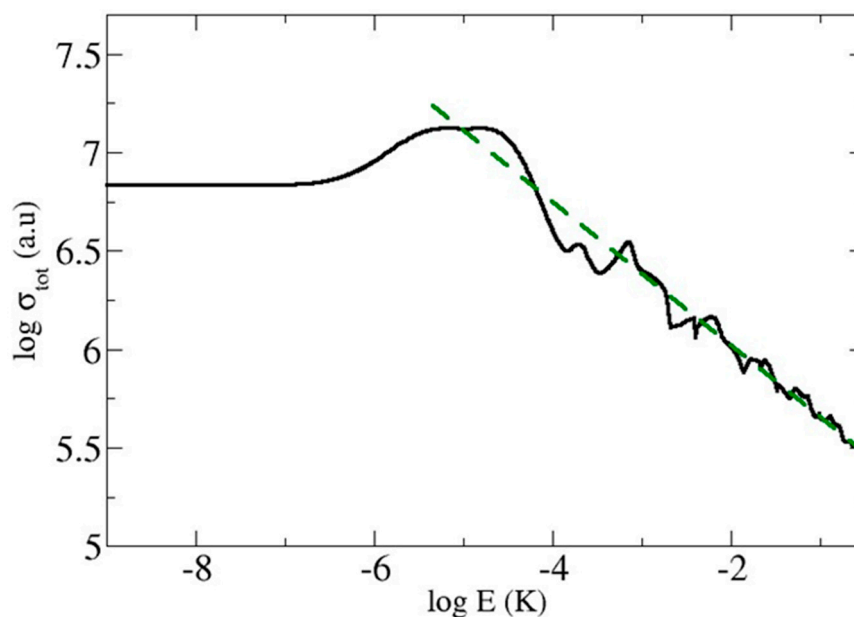


Figure 7. Logarithm of total elastic scattering cross-sections (σ_{tot}) in a.u. as a function of logarithm energy E of the (MgCs)⁺ molecular ion.

In our calculations, we have included 70 partial waves, since, with the increase in energy, large numbers of partial waves start to contribute to the total elastic scattering cross-section. Considering the logarithm on both sides of Equation (8), a straight line is obtained with a slope equal to $-1/3$. From the linear fitting of $\log \sigma_{tot}$ vs. $\log E$ of Figure 7, we have verified the numerically calculated slope of the straight line is quite close to the theoretical value.

2.1.6. Two-Photon Photoassociation: Molecular Ion Formation

In this section, we explore the molecular ion formation in the ground-state electronic potential $X^1\Sigma^+$ by a two-photon incoherent Raman process in the presence of two applied lasers, L_1 and L_2 , respectively. The formation of the molecular ion needs two steps. Initially, the atom-ion pair present in the ground-state scattering continuum ($X^1\Sigma^+$) is irradiated

with laser L_1 with a suitable frequency to form the molecular ion in one of the bound levels of the first excited potential $2^1\Sigma^+$. Once the molecular ion is formed, laser L_2 is turned on to de-excite the molecular ion to the ground electronic potential followed by bound-bound transition.

Here, the rate coefficient of the first step concerned, which is known as single-photon photoassociation (PA) at a temperature T , is given by [78]

$$K_{PA} = \left\langle \frac{\pi v_{rel}}{k^2} \sum_{l=0}^{\infty} (2l+1) |S_{PA}(E, l, \omega_l)|^2 \right\rangle \quad (9)$$

where v_{rel} is the relative velocity of the interacting particles, S_{PA} is the scattering matrix element, and $\langle \dots \rangle$ implies an averaging over thermal velocity distribution. At a very low-temperature limit, the energy of the interacting particle is such that their dynamics may be described by the s -wave scattering. If one considers a Maxwellian velocity distribution of an ultracold mixture of gas, Equation (9) can be represented as

$$K_{PA}(T, \omega_L) = \frac{1}{hQ_T} \sum_{l=0}^{\infty} (2l+1) \int_0^{\infty} |S_{PA}(E, l, \omega_L)|^2 e^{-\beta E} dE \quad (10)$$

Here, $Q_T = (2\pi\mu k_B T/h^2)^{3/2}$ is the translational partition function, $\beta = 1/k_B T$, and k_B is the Boltzmann constant. The scattering S -matrix element is given by

$$|S_{PA}|^2 = \frac{\gamma_s \Gamma_l}{\delta_E^2 + (\gamma/2)^2} \quad (11)$$

The scattering phase shift (η) is related to the scattering T -matrix as $T = \frac{1-e^{2i\eta}}{2i} = -e^{i\eta} \sin \eta$, while the quantity $|T|^2 = \sin^2 \eta$. Again, the scattering S -matrix is related to the T -matrix as $S = 1 - 2iT$ and the quantity $|S|^2 = 1 + 4 \sin^2 \eta$. Therefore, in terms of phase shift and T -matrix, Equation (11) becomes

$$|T|^2 = \sin^2 \eta = \frac{1}{4} \left[\frac{\gamma_s \Gamma_l}{\delta_E^2 + (\gamma/2)^2} - 1 \right] \quad (12)$$

where detuning parameters are defined as $\delta_E = \frac{E}{\hbar} + \delta_{v,j}$, $\delta_{v,j} = \omega_L - \omega_{v,j}$ with $E_{v,j} = \hbar\omega_{v,j}$ is the binding energy of the excited co-vibrational state, ω_L is the frequency of the applied laser L_1 . Here, γ_s is the spontaneous line width, and Γ_l is the stimulated line width. We consider that other decay processes, such as molecular predissociation, are either negligible or not present in our system.

The PA rate is determined, basically, by stimulated line width and can be expressed by the Golden rule as

$$\Gamma_l = \frac{\pi I}{\epsilon_0 c} |\langle \phi_{v,j} | D(r) | \psi_l(kr) \rangle|^2 \quad (13)$$

We termed the quantity $D_{v,j,l} = \langle \phi_{v,j} | D(r) | \psi_l(kr) \rangle$ as the radial transition dipole matrix element between the unit normalized bound state wave function $\phi_{v,j}$ and energy normalized continuum wave function $\psi_l(kr)$, and $D(r)$ is the transition dipole moment. Here, I is the intensity of the laser L_1 , c is the velocity of light, and ϵ_0 is the vacuum permittivity.

In order to calculate the quantity $D_{v,j,l}$ for the optimal production of molecular ions by the PA process, we have to calculate the scattering state and suitable bound state wave functions. We solve the partial-wave Schrödinger Equation (6) by standard renormalized Numerov-Cooley method [78] for the determination of the wave functions that we discussed. In general, molecular dipole transitions between two bound states or between continuum and bound states are controlled by the FC principle. The free-bound FC value is highest for the bound state $\phi_{v,j}$ ($v = 17, j = 1$) of the first excited potential $2^1\Sigma^+$ of $(\text{MgCs})^+$ system. The PA rate coefficient is calculated according to Equation (9) to form the molecular

ion in the excited electronic state $2^1\Sigma^+$. In Figure 8, we have shown the rate coefficient of PA as a function of energy E (in Kelvin), considering the atom–ion pairs Mg–Cs⁺ are initially lying in the ground-state scattering continuum. We considered the laser intensity $L_1 = 10 \text{ W/cm}^2$ tuned at the PA resonance. We find that our calculated PA rate coefficient is consistent with the results of Li⁺-Be [79] and K⁺-Mg [49] systems. Finally, in Figure 9, we have shown the variation of the rate of ion–atom PA as a function of the intensity of the applied laser L_1 considering the temperature at $10 \mu\text{K}$. We have observed that a saturation effect on the ion–atom PA rate occurs near the laser intensity $I = 35 \text{ kW/cm}^2$.

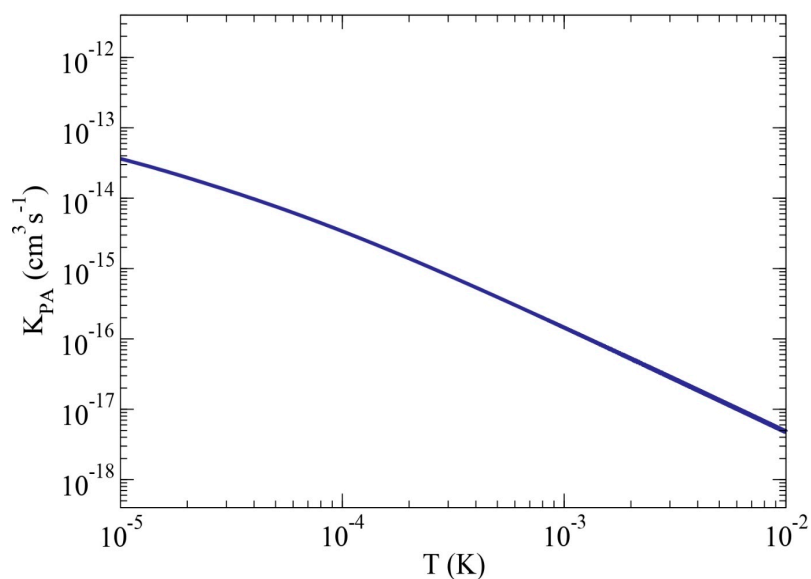


Figure 8. The rate constant $K_{PA} \text{ (cm}^3\text{s}^{-1}\text{)}$ of PA as a function of energy E (in Kelvin) for laser frequency 10 W/cm^2 tuned at PA resonance.

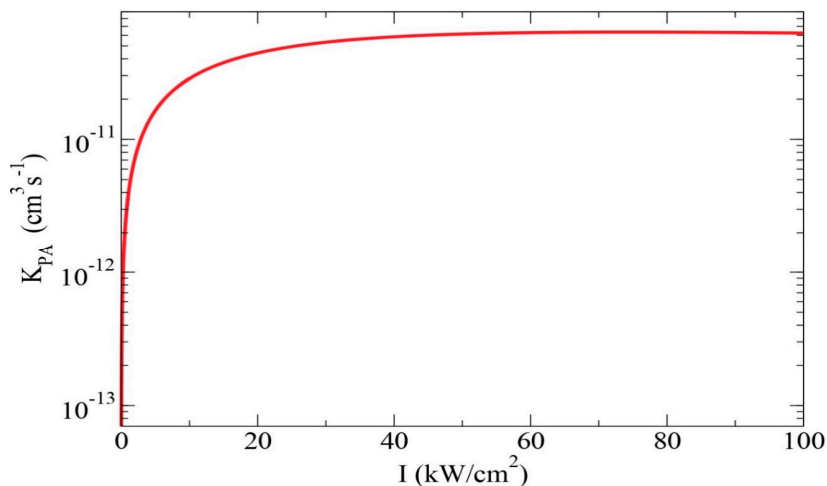


Figure 9. The variation of the rate constant of photoassociation as a function of the intensity of the applied laser.

Now we discuss the formation of a ground-state molecular ion by stimulated Raman-type process in the presence of a second applied laser L_2 tuned near a bound–bound transition between the potentials $2^1\Sigma^+$ and $X^1\Sigma^+$, respectively. To find the efficacy of the coherent laser coupling between the two bound states, we calculate the Rabi coupling Ω given by

$$\hbar\Omega = \left(\frac{I}{4\pi c\epsilon_0} \right)^{1/2} \left| \langle \phi_{v,j} | D(r) \cdot \epsilon | \phi_{v',j'} \rangle \right| \tag{14}$$

where I is the intensity of the second applied laser L_2 tuned to the transition frequency, ϵ is the unit vector of laser polarization, and $\phi_{v,j}$ and $\phi_{v',j'}$ are the two bound states of excited ($2^1\Sigma^+$) and ground ($X^1\Sigma^+$) state electronic potentials, respectively. We have calculated the Rabi frequencies between the selected bound state ($v = 15, j = 1$) of the first excited molecular potential and different bound states of the ground electronic potential, considering an intensity of laser $L_2 = 10 \text{ kW/cm}^{-2}$. We observed that the bound-bound Rabi coupling is maximum ($\Omega = 150 \text{ MHz}$) for the bound state $\phi_{v',j'}(v'=16, j' = 0)$ of $X^1\Sigma^+$ potential. Comparing this value with the spontaneous line width ($\gamma = 120 \text{ kHz}$) of the excited bound state calculated using the formula [80], we found that bound-bound Rabi coupling (Ω) is several orders of magnitude higher. Therefore, we may infer that the ground-state molecular ion formation is likely to be possible by a stimulated Raman-type process [49,80,81].

3. Conclusions

In this work, an extended and complete study devoted to the $(\text{MgCs})^+$ molecular ion was presented. We have performed precise ab initio calculations for the potential energy curves and their related spectroscopic constants for the ground and the 20 low-lying excited states of $^{1,3}\Sigma^+$ symmetries below the $\text{Mg}^{2+}\text{Cs}^-$ asymptotic limit.

The computational method used is based on a non-empirical pseudo-potential approach for Mg^{2+} and Cs^+ cores, which allows treating the ionic molecule as a two-electron system where full configuration interaction FCI calculations can be easily performed. An interesting series of avoided crossings have been observed between the same symmetry of the $^{1,3}\Sigma^+$ states. These avoided crossings often lead to relatively irregular dipole moment curves, which are both manifestations of abrupt changes in the character of the electronic wave functions with underlying strong interactions between the electronic states. These interactions could give rise to important charge transfer for collisions between the atom-ion combinations. In addition, the vibrational levels and their spacings were investigated for all attractive states. Finally, electric permanent and transition dipole moments were calculated. As expected, the permanent dipole moments of the electronic states dissociating into $\text{Mg} \{(3s^2 (^1S), 3s3p (^3P), 3s3p (^1P), 3s4s (^3S), 3s4s (^1S), 3s3d (^1D), 3s4p (^3P), 3s3d (^3D), (^1P), 3s5s (^3S), 3s5s (^1S), 3s4d (^1D), 3s4d (^3D), \text{ and } 3s5p (^3P))\} + \text{Cs}^+$ have shown an almost linear features function of R , especially for intermediate and large internuclear distances. Moreover, the abrupt changes in the permanent dipole moment are localized at particular distances corresponding to the avoided crossings between the two neighboring electronic states.

In this study, the ab initio calculations were carefully performed to produce accurate data, even though there is a lack of experimental studies for this molecular ion. However, theoretically, only the ground state of $(\text{MgCs})^+$ was studied in a recent work published by Smialkowski and Tomza [28]. We expect that our data can serve as a solid foundation for future and advanced dynamic studies for the $(\text{MgCs})^+$ molecular ion.

These precise data were then used for elastic diffusion calculations between Mg and Cs^+ at low temperatures. In fact, a theoretical understanding of low-energy atom-ion scattering can help probe the dynamics of quantum gases. Furthermore, we theoretically predict the formation of a cold molecular ion in translation and rotation by an incoherent two-photon Raman process. The formation of such cold molecular ions is very important in the research domain of ultracold chemistry and precision spectroscopy. Our data can be used to understand several phenomena, like charge transfer, diffusion, and partial-wave phase locking, and is comparable with the recently studied Li-Ba^+ system [81]. We believe that our analysis, including the ab initio data, may serve as a solid platform for future study on $(\text{MgCs})^+$ molecular ionic systems.

Author Contributions: Conceptualization, H.B., M.F., D.S. and B.D.; Methodology, H.B., M.F., D.S. and B.D.; Investigation, M.F. and D.S.; Writing-original draft preparation, M.F. and D.S.; Writing-review and editing, H.B., M.F. and D.S. All authors have read and agreed to the published version of the manuscript.

Funding: H.B. would like to acknowledge the financial support of the American University of Ras Al Khaimah under seed grant no. AAS/003/21.

Data Availability Statement: Not applicable.

Acknowledgments: H.B. would like to acknowledge the financial support of the American University of Ras Al Khaimah under seed grant no. AAS/003/21.

Conflicts of Interest: The authors declare no conflict of interest. The funders had no role in the design of the study; in the collection, analyses, or interpretation of data; in the writing of the manuscript; or in the decision to publish the results.

References

1. Carr, L.D.; DeMille, D.; Krems, R.V.; Ye, J. Cold and ultracold molecules: Science, technology and applications. *New J. Phys.* **2009**, *11*, 055049. [[CrossRef](#)]
2. Hummon, M.T.; Yeo, M.; Stuhl, B.K.; Collopy, A.L.; Xia, Y.; Ye, J. 2D Magneto-Optical Trapping of Diatomic Molecules. *Phys. Rev. Lett.* **2013**, *110*, 143001. [[CrossRef](#)] [[PubMed](#)]
3. Stwalleyand, W.C.; Wang, H. Photoassociation of Ultracold Atoms: A New Spectroscopic Technique. *J. Mol. Spectrosc.* **1999**, *195*, 194. [[CrossRef](#)] [[PubMed](#)]
4. Côté, R.; Dalgarno, A. Ultracold atom-ion collisions. *Phys. Rev. A* **2000**, *62*, 012709. [[CrossRef](#)]
5. Idziaszek, Z.; Calarco, T.; Julienne, P.S.; Simoni, A. Quantum theory of ultracold atom-ion collisions. *Phys. Rev. A* **2009**, *79*, 010702. [[CrossRef](#)]
6. Krych, M.; Skomorowski, W.; Pawłowski, F.; Moszynski, R.; Idziaszek, Z. Sympathetic cooling of the Ba⁺ ion by collisions with ultracold Rb atoms: Theoretical prospects. *Phys. Rev. A* **2011**, *83*, 032723. [[CrossRef](#)]
7. Ravi, K.; Lee, S.; Sharma, A.; Werth, G.; Rangwala, S. Cooling and stabilization by collisions in a mixed ion-atom system. *Nat. Commun.* **2012**, *3*, 1126. [[CrossRef](#)] [[PubMed](#)]
8. Sivarajah, I.; Goodman, D.S.; Wells, J.E.; Narducci, F.A.; Smith, W.W. Evidence of sympathetic cooling of Na⁺ ions by a Na magneto-optical trap in a hybrid trap. *Phys. Rev. A* **2012**, *86*, 063419. [[CrossRef](#)]
9. Boyarkin, O.V.; Mercier, S.R.; Kamariotis, A.; Rizzo, T.R. Electronic spectroscopy of cold, protonated tryptophan and tyrosine. *J. Am. Chem. Soc.* **2006**, *128*, 2816–2817. [[CrossRef](#)]
10. Willitsch, S.; Bell, T.M.; Gingell, A.D.; Procter, S.R.; Softley, T.P. Cold Reactive Collisions between Laser-Cooled Ions and Velocity-Selected Neutral Molecules. *Phys. Rev. Lett.* **2008**, *100*, 043203. [[CrossRef](#)]
11. Schmid, S.; Härter, A.; Denschlag, J.H. Dynamics of a Cold Trapped Ion in a Bose-Einstein Condensate. *Phys. Rev. Lett.* **2010**, *105*, 133202. [[CrossRef](#)] [[PubMed](#)]
12. Jones, K.M.; Tiesinga, E.; Lett, P.D.; Julienne, P.S. Ultracold photoassociation spectroscopy: Long-range molecules and atomic scattering. *Rev. Mod. Phys.* **2006**, *78*, 483. [[CrossRef](#)]
13. Chin, C.; Grimm, R.; Julienne, P.; Tiesinga, E. Feshbach resonances in ultracold gases. *Rev. Mod. Phys.* **2010**, *82*, 1225–1286. [[CrossRef](#)]
14. Da Silva, H., Jr.; Raoult, M.; Aymar, M.; Dulieu, O. Formation of molecular ions by radiative association of cold trapped atoms and ions. *New J. Phys.* **2015**, *17*, 045015. [[CrossRef](#)]
15. Hall, F.H.J.; Aymar, M.; Bouloufa-Maafa, N.; Dulieu, O.; Willitsch, S. Light-Assisted Ion-Neutral Reactive Processes in the Cold Regime: Radiative Molecule Formation versus Charge Exchange. *Phys. Rev. Lett.* **2011**, *107*, 243202. [[CrossRef](#)] [[PubMed](#)]
16. Hall, F.H.; Eberle, P.; Hegi, G.; Raoult, M.; Aymar, M.; Dulie, O.; Willitsch, S. Formation of molecular ions by radiative association of cold trapped atoms and ions. *Mol. Phys.* **2013**, *111*, 2020. [[CrossRef](#)]
17. Mohammadi, A.; Krüchow, A.; Mahdian, A.; Deiß, M.; Pérez-Ríos, J., Jr.; da Silva, H. Life and death of a cold BaRb⁺ molecule inside an ultracold cloud of Rb atoms. *Phys. Rev. Res.* **2021**, *3*, 013196. [[CrossRef](#)]
18. Schmid, S.; Härter, A.; Frisch, A.; Hoinka, S.; Denschlag, J.H. An apparatus for immersing trapped ions into an ultracold gas of neutral atoms. *Rev. Sci. Instrum.* **2012**, *83*, 053108. [[CrossRef](#)]
19. Baba, T.B.T.; Waki, I.W.I. Cooling and Mass-Analysis of Molecules Using Laser-Cooled Atoms. *Jpn. J. Appl. Phys.* **1996**, *35*, L1134. [[CrossRef](#)]
20. Bertelsen, A.; Vogelius, I.S.; Jørgensen, S.; Kosloff, R.; Drewsen, M. Photo-dissociation of Cold MgH⁺ ions. *Eur. Phys. J. D* **2004**, *31*, 403. [[CrossRef](#)]
21. Mølhave, K.; Drewsen, M. Formation of translationally cold MgH⁺ and MgD⁺ molecules in an ion trap. *Phys. Rev. A* **2000**, *62*, 011401. [[CrossRef](#)]
22. Aymar, M.; Guérout, R.; Sahlaoui, M.; Dulieu, O. Electronic structure of the magnesium hydride molecular ion. *J. Phys. B: At. Mol. Opt. Phys.* **2009**, *42*, 154025. [[CrossRef](#)]
23. Khemiri, N.; Dardouri, R.; Oujia, B.; Gadéa, F.X. Ab Initio Investigation of Electronic Properties of the Magnesium Hydride Molecular Ion. *J. Phys. Chem. A* **2013**, *117*, 8915–8924. [[CrossRef](#)] [[PubMed](#)]
24. Boldyrev, A.I.; Simons, J.; von, R. Schleyer, P. Ab initio study of the electronic structures of lithium containing diatomic molecules and ions. *J. Chem. Phys.* **1993**, *99*, 8793–8804. [[CrossRef](#)]

25. Pekka Pyykk, Ö. Ab initio study of bonding trends among the 14-electron diatomic systems: From B_2^{4+} to F_2^{4+} . *Mol. Phys.* **1989**, *67*, 871. [[CrossRef](#)]
26. Gao, Y.; Gao, T. Ab initio study of ground and low-lying excited states of MgLi and MgLi⁺ molecules with valence full configuration interaction and MRCI method. *Mol. Phys.* **2014**, *112*, 3015. [[CrossRef](#)]
27. Fedorov, D.A.; Barnes, D.K.; Varganova, S.A. Ab initio calculations of spectroscopic constants and vibrational state lifetimes of diatomic alkali-alkaline-earth cations. *J. Chem. Phys.* **2017**, *147*, 124304. [[CrossRef](#)] [[PubMed](#)]
28. Smialkowski, M.; Tomza, M. Interactions and chemical reactions in ionic alkali-metal and alkaline-earth-metal diatomic AB⁺ and triatomic A₂B⁺ systems. *Phys. Rev. A* **2020**, *101*, 012501. [[CrossRef](#)]
29. ElOualhazi, R.; Berriche, H. Electronic Structure and Spectra of the MgLi⁺ Ionic Molecule. *J. Phys. Chem. A* **2016**, *120*, 452. [[CrossRef](#)]
30. Bala, R.; Nataraj, H.S.; Abe, M.; Kajita, M. Calculations of electronic properties and vibrational parameters of alkaline-earth lithides: MgLi⁺ and CaLi⁺. *Mol. Phys.* **2018**, *117*, 712–725. [[CrossRef](#)]
31. Grier, A.T.; Cetina, M.; Oručević, F.; Vuletić, V. Observation of Cold Collisions between Trapped Ions and Trapped Atoms. *Phys. Rev. Lett.* **2009**, *102*, 223201. [[CrossRef](#)]
32. Sullivan, S.T.; Rellergert, W.G.; Kotochigova, S.; Hudson, E.R. Role of Electronic Excitations in Ground-State-Forbidden Inelastic Collisions Between Ultracold Atoms and Ions. *Phys. Rev. Lett.* **2012**, *109*, 223002. [[CrossRef](#)]
33. Rellergert, W.G.; Sullivan, S.T.; Kotochigova, A.; Petrov, K.S.; Chen, S.; Schowalter, J.; Hudson, E.R.; Millikelvin, E. Reactive Collisions between Sympathetically Cooled Molecular Ions and Laser-Cooled Atoms in an Ion-Atom Hybrid Trap. *Phys. Rev. Lett.* **2011**, *107*, 24320.
34. Zipkes, C.; Palzer, S.; Sias, C.; Köhl, M. A trapped single ion inside a Bose–Einstein condensate. *Nature* **2010**, *464*, 388–391. [[CrossRef](#)]
35. Haze, S.; Hata, S.; Fujinaga, M.; Mukaiyama, T. Observation of elastic collisions between lithium atoms and calcium ions. *Phys. Rev. A* **2013**, *87*, 052715. [[CrossRef](#)]
36. Smith, W.; Goodman, D.; Sivarajah, I.; Wells, J.; Banerjee, S.; Côté, R.; Michels, H.; Montgomery, J.A.; Narducci, F. Experiments with an ion-neutral hybrid trap: Cold charge-exchange collisions. *Appl. Phys. B* **2014**, *114*, 75. [[CrossRef](#)]
37. Meir, Z.; Sikorsky, T.; Ben-Shlomi, R.; Akerman, N.; Dallal, Y.; Ozeri, R. Dynamics of a Ground-State Cooled Ion Colliding with Ultracold Atoms. *Phys. Rev. Lett.* **2016**, *117*, 243401. [[CrossRef](#)] [[PubMed](#)]
38. Fürst, H.; Feldker, T.; Ewald, N.V.; Joger, J.; Tomza, M.; Gerritsma, R. Dynamics of a single ion-spin impurity in a spin-polarized atomic bath. *Phys. Rev. A* **2018**, *98*, 012713. [[CrossRef](#)]
39. yothi, S.; Egodapitiya, K.N.; Bondurant, B.; Jia, Z.; Pretzsch, E.; Chiappina, P.; Shu, G.; Brown, K.R. A hybrid ion-atom trap with integrated high resolution mass spectrometer. *Rev. Sci. Instruments* **2019**, *90*, 103201.
40. Schmidt, J.; Weckesser, P.; Thielemann, F.; Schaetz, T.; Karpa, L. Optical Traps for Sympathetic Cooling of Ions with Ultracold Neutral Atoms. *Phys. Rev. Lett.* **2020**, *124*, 053402. [[CrossRef](#)]
41. Härter, A.; Krüchow, A.; Brunner, A.; Schnitzler, W.; Schmid, S.; Denschlag, J.H. Single Ion as a Three-Body Reaction Center in an Ultracold Atomic Gas. *Phys. Rev. Lett.* **2012**, *109*, 123201. [[CrossRef](#)]
42. Jyothi, S.; Ray, T.; Dutta, S.; Allouche, A.R.; Vexiau, R.; Dulieu, O.; Rangwala, S.A. Photodissociation of Trapped Rb⁺²: Implications for Simultaneous Trapping of Atoms and Molecular Ions. *Phys. Rev. Lett.* **2016**, *117*, 213002. [[CrossRef](#)] [[PubMed](#)]
43. da Silva, H., Jr.; Raoult, M.; Aymar, M.; Dulieu, O. Formation of molecular ions by radiative association of cold trapped atoms and ions. *Mol. Phys.* **2013**, *111*, 1683. [[CrossRef](#)]
44. Alharzali, N.; Sardar, D.; Mlika, R.; Deb, B.; Berriche, H. Spectroscopic properties and cold elastic collisions of alkaline-earth Mg + Mg⁺ system. *J. Phys. B At. Mol. Opt. Phys.* **2018**, *51*, 195201. [[CrossRef](#)]
45. Singer, K.; Poschinger, U.; Murphy, M.; Ivanov, P.; Ziesel, F.; Calarco, T.; Schmidt-Kaler, F. Trapped ions as quantum bits: Essential numerical tools. *Rev. Mod. Phys.* **2010**, *82*, 2609–2632. [[CrossRef](#)]
46. Schneider, C.; Porras, D.; Schaetz, T. Experimental quantum simulations of many-body physics with trapped ions. *Rep. Prog. Phys.* **2012**, *75*, 024401. [[CrossRef](#)] [[PubMed](#)]
47. Idziaszek, Z.; Simoni, A.; Calarco, T.; Julienne, P.S. Multichannel quantum-defect theory for ultracold atom–ion collisions. *New J. Phys.* **2011**, *13*, 083005. [[CrossRef](#)]
48. Tomza, M.; Koch, C.P.; Moszynski, R. Quantum gas microscopy with spin, atom-number, and multilayer readout. *Phys. Rev. A* **2015**, *91*, 042706. [[CrossRef](#)]
49. Farjallah, M.; Sardar, D.; El-Kork, N.; Deb, B.; Berriche, H. Electronic structure and photoassociation scheme of ultracold (MgK⁺) molecular ions. *J. Phys. B At. Mol. Opt. Phys.* **2018**, *52*, 045201. [[CrossRef](#)]
50. Gacesa, M.; Montgomery, J.A.; Michels, H.H.; Côté, R. Controlling charge transfer in ultracold gases via Feshbach resonances. *Phys. Rev. A* **2016**, *94*, 013407. [[CrossRef](#)]
51. Petrov, A.; Makrides, C.; Kotochigova, S.J. A new approach to molecular dynamics with non-adiabatic and spin-orbit effects with applications to QM/MM simulations of thiophene and selenophene. *Chem. Phys.* **2017**, *146*, 08430.
52. Zrafi, W.; Ladjimi, H.; Said, H.; Berriche, H.; Tomza, M. Ab initio electronic structure and prospects for the formation of ultracold calcium–alkali-metal-atom molecular ions. *New J. Phys.* **2020**, *22*, 073015. [[CrossRef](#)]
53. Ladjimi, H.; Farjallah, M.; Berriche, H. Spectroscopic, structural and lifetime calculations of the ground and low-lying excited states of the BeNa⁺, BeK⁺, and BeRb⁺ molecular ions. *Phys. Scrip.* **2020**, *95*, 055404. [[CrossRef](#)]

54. Ladjimi, H.; Sardar, D.; Farjallah, M.; Alharzali, N.; Naskar, S.; Mlika, R.; Berriche, H.; Deb, B. Spectroscopic properties of the molecular ions BeX^+ ($X = \text{Na}, \text{K}, \text{Rb}$): Forming cold molecular ions from an ion–atom mixture by stimulated Raman adiabatic process. *Mol. Phys.* **2018**, *116*, 1812–1826. [[CrossRef](#)]
55. Ladjimi, H.; Zrafi, W.; Farjallah, M.; Bejaoui, M.; Berriche, H. Electronic structure, cold ion–atom elastic collision properties and possibility of laser cooling of BeCs^+ molecular ion. *Phys. Chem. Chem. Phys.* **2022**, *24*, 18511–18522. [[CrossRef](#)] [[PubMed](#)]
56. Ghanmi, C.; Farjallah, M.; Berriche, H. Theoretical study of the alkaline-earth $(\text{LiBe})^+$ ion: Structure, spectroscopy and dipole moments. *J. Phys. B* **2017**, *50*, 055101. [[CrossRef](#)]
57. Farjallah, M.; Ghanmi, C.; Berriche, H. Structure and spectroscopic properties of the beryllium hydride ion BeH^+ : Potential energy curves, spectroscopic constants, vibrational levels and permanent dipole moments. *Eur. Phys. J. D* **2013**, *67*, 245. [[CrossRef](#)]
58. Evangelisti, S.; Daudey, J.-P.; Malrieu, J.-P. Convergence of an improved CIPSI algorithm. *Chem. Phys.* **1983**, *75*, 91–102. [[CrossRef](#)]
59. Durand, P.; Barthelat, J.C. A theoretical method to determine atomic pseudopotentials for electronic structure calculations of molecules and solids. *Theor. Chim. Acta* **1975**, *38*, 283–302. [[CrossRef](#)]
60. Durand, P.; Barthelat, J.C. Pseudopotentials in atomic and molecular physics. *Chem. Gazz. Chim. Ital.* **1978**, *108*, 225–236.
61. Barthelat, J.C.; Durand, P.; Serafini, A. Non-empirical pseudopotentials for molecular calculations. *Mol. Phys.* **1977**, *33*, 159–180. [[CrossRef](#)]
62. Müller, W.; Flesch, J.; Meyer, W. Treatment of intershell correlation effects in ab initio calculations by use of core polarization potentials. Method and application to alkali and alkaline earth atoms. *J. Chem. Phys.* **1984**, *80*, 3297–3310. [[CrossRef](#)]
63. Foucrault, M.; Millié, P.; Daudey, J.P. Non-perturbative method for core–valence correlation in pseudopotential calculations: Application to the Rb_2 and Cs_2 molecules. *J. Chem. Phys.* **1992**, *96*, 1257–1264. [[CrossRef](#)]
64. Wilson, J.N.; Curtis, R.M. Dipole polarizabilities of ions in alkali halide crystals. *J. Phys. Chem.* **1970**, *74*, 187–196. [[CrossRef](#)]
65. Pavolini, D.; Gustavsson, T.; Spiegelmann, F.; Daudey, J.P. Theoretical study of the excited states of the heavier alkali dimers. I. The RbCs molecule. *J. Phys. B Mol. Opt.* **1989**, *77*, 221721. [[CrossRef](#)]
66. Ghanmi, C.; Berriche, H.; Ben Ouada, H. Evaluation of the Atomic Polarisabilities of Li and K using the Long Range Li^+ Electronic States Behaviour. In Proceedings of the International Conference on Computational and Mathematical Methods in Science and Engineering, CMMSE, Alicante, Spain, 27–30 June 2005; pp. 166–174.
67. Bouzouita, H.; Ghanmi, C.; Berriche, H. Ab initio study of the alkali-dimer cation Li_2^+ . *J. Mol. Struct. Theochem.* **2006**, *777*, 75–80. [[CrossRef](#)]
68. Moore, C.E.; Mack, J.E. Atomic energy levels. *At. Energy Levels Deriv. Anal. Opt. Spectra. Phys. Today* **1952**, *5*, 23. [[CrossRef](#)]
69. Mitroy, J.; Zhang, J.Y. Long range interactions of the Mg^+ and Ca^+ ions. *Eur. Phys. J. D* **2007**, *46*, 415–424. [[CrossRef](#)]
70. Moore, C.E. *Atomic Energy Levels*; NSRDS-NBS No. 467; US Government Printing Office: Washington, DC, USA, 1989.
71. Zemke, W.T.; Crooks, J.B.; Stwalley, W.C. Radiative and nonradiative lifetimes for vibrational levels of the $A^1\Sigma^+$ state of ^7LiH . *J. Chem. Phys.* **1978**, *68*, 4628. [[CrossRef](#)]
72. Partridge, H.; Langhoff, S.R. Theoretical treatment of the $X^1\Sigma^+$, $A^1\Sigma^+$, and $B^1\Pi$ states of LiH . *J. Chem. Phys.* **1981**, *74*, 2361. [[CrossRef](#)]
73. Berriche, H.; Gadéa, F.X. Transition dipole function and radiative lifetimes for the A and C $^1\Sigma^+$ states of the LiH molecule. *Eur. Phys. J. D* **2016**, *70*, 1–9. [[CrossRef](#)]
74. Berriche, H. Ab Initio Adiabatic and Diabatic Permanent Dipoles for the Low-Lying States of the LiH Molecule. Ph.D. Thesis, Paul Sabatier University, Toulouse, France, 1995.
75. Stolyarov, A.V.; Pupyshv, V.I. Approximate sum rule for diatomic vibronic states. *Phys. Rev. A* **1994**, *49*, 1693. [[CrossRef](#)]
76. Pazyuk, E.; Stolyarov, A.; Pupyshv, V. Approximate sum rule for diatomic vibronic states as a tool for the evaluation of molecular properties. *Chem. Phys. Lett.* **1994**, *228*, 219–224. [[CrossRef](#)]
77. Johnson, R.B. New numerical methods applied to solving the one-dimensional eigenvalue problem. *J. Chem. Phys.* **1977**, *67*, 4086. [[CrossRef](#)]
78. Napolitano, R.; Weiner, J.; Williams, C.J.; Julienne, P.S. Line Shapes of High Resolution Photoassociation Spectra of Optically Cooled Atoms. *Phys. Rev. Lett.* **1994**, *73*, 1352–1355. [[CrossRef](#)] [[PubMed](#)]
79. Rakshit, A.; Deb, B. Formation of cold molecular ions by radiative processes in cold ion-atom collisions. *Phys. Rev. A* **2011**, *83*, 022703. [[CrossRef](#)]
80. Sardar, D.; Naskar, S.; Pal, A.; Berriche, H.; Deb, B. Formation of a molecular ion by photoassociative Raman processes. *J. Phys. B At. Mol. Opt. Phys.* **2016**, *49*, 245202. [[CrossRef](#)]
81. Sardar, D.; Naskar, S. Cold collisions between alkali metals and alkaline-earth metals in the heteronuclear atom-ion system $\text{Li} + \text{Ba}^+$. *Phys. Rev. A* **2023**, *107*, 043323. [[CrossRef](#)]

Disclaimer/Publisher’s Note: The statements, opinions and data contained in all publications are solely those of the individual author(s) and contributor(s) and not of MDPI and/or the editor(s). MDPI and/or the editor(s) disclaim responsibility for any injury to people or property resulting from any ideas, methods, instructions or products referred to in the content.